Chapter 7. Fracture Energy of CNT/Epoxy Nanocomposites with Progressive Interphase Debonding, Cavitation, and Plastic Deformation of Nanovoids

The contents of this chapter have appeared as:

A. Tiwari, S.K. Panda, Fracture energy of CNT/epoxy nanocomposites with progressive interphase debonding, cavitation, and plastic deformation of nanovoids, ***Fatigue Fract. Eng. Mater. Struct***. 46 (2023) 1170-1189.https://doi.org/10.1111/ffe.13929.

7.1.Introduction

CNT are known to be excellent nanoparticles for reinforcement in epoxy due to their unique atomic structure, very high aspect ratio and unique mechanical properties[66]. The prospect of improving material properties such as stiffness and strength of epoxy resin with CNT reinforcement has been reported by researcher[67]. Experimental evidence has also shown that CNT significantly enhances the fracture toughness of epoxy[69,70]. Moreover, the study of fracture toughness was also carried out with theoretical models. The molecular dynamic method was also applied for fracture toughness analysis[71]. Mirjalili [68] suggested that the orientation of CNT influenced the Mode I toughness of nanocomposite and derived a model based on the elastic-plastic fracture mechanics. A certain preparatory analysis in this direction considering CNT debonding has already been described by Shokrieh [72]. They reported that interphase properties and CNT weight fraction influence the fracture toughness characteristics of the nanocomposite system. However, similar studies in this direction lack to take into account the multi-phase mechanism involving the multi-scale physical constituents at nano-scale, microscale and macroscale, affecting the debonding progression, void formation and subsequent plastic deformation along the CNT/interphase/matrix interface. In the light of above discussions, the key objectives of the present work have been stated as follows:

- The multi-scale modelling procedure has been adopted to evaluate the overall fracture toughness improvement of CNT-reinforced nanocomposite considering the debonding mechanism, elastic cavitation and plastic deformation of nanovoids.
- Identification of the most influential mechanism among the stated three causes and their relative severity towards fracture mode enhancement
- Influence of interphase geometric and material parameters on the distribution of normalized energy release rate as a fracture parameter
- Assessment and comparison of fracture characteristics for different moduli ratio of interphase and matrix, the thickness of interphase and hardening coefficient of plastic yielding

The multi-scale model for elastic cavitation and plastic deformation of nanovoids surrounding crack tips under open-mode loading is derived from the correlation among the nano, micro, and macro scales stress distributions. In the development of the model, a cylindrical RVE, which successively consists of CNT at the core, the interphase, and then neat resin at the outer surface, is utilized for investigating the stress and displacement correlation. The debonding stress and fracture toughness are described as a function of the variables, such as CNT weight fraction, interphase thickness between the matrix and CNT, and mechanical properties of each constituent of the RVE.

7.2.A theoretical multi-scale modelling approach

7.2.1. General concepts

Modelling of nanocomposite is endowed with three successive scales, viz. nano, micro, and macro scale, each designated by Eshelby [253,254], Mori-Tanaka [255] and Norris [256] distinctive circumstances and magnitudes at their respective scale. The bridging of the influence of each scale from the nano- to the micro- and the micro- to the macro-scale can be described by the correlation of macro, micro, and nano-scale stress system **Fig. 7.1**. The effective properties of these materials are predicted following the same correlations. The constitutive equation for each phase of a Ω-phase homogeneous nanocomposite is defined below[257].

$$\sigma^{\Omega} = C^{\Omega}\varepsilon^{\Omega} \tag{7.1}$$

where σ^{Ω} , C^{Ω}, and ε^{Ω} are the stress, stiffness, and strain tensors in the Ω^{th} phase (i.e., CNT, interphase and matrix) homogeneous nanocomposite, respectively. The surface of a homogeneous body will form a homogeneous field if homogeneous boundary conditions are imposed.

Depending on the scale of representation, the material constitutive relation can be described. For example:

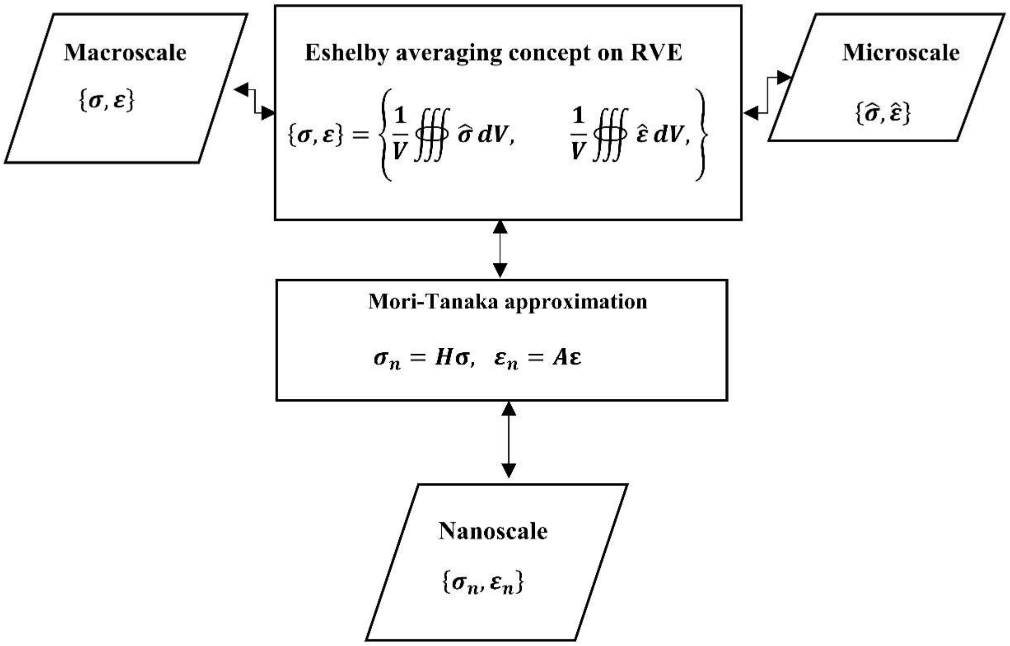

Fig. 7.1 Correlation of macro, micro, and nanoscale stress system

7.2.1.1. Macro-scale:

At the macroscale, the distribution of material is assumed to be homogeneous and continuous, So the smallest element of the material possesses the homological specified physical properties. The material system under this presumption having uniformly distributed and randomly oriented nanoparticles can also be considered isotropic without any loss of generalization. All the material's physical properties (such as elastic moduli) are calculated as averaged magnitudes [258] and assumed to be representative of the entire material behaviour.

7.2.1.2. Micro-scale:

The micro-scale is mainly referred to the adequately small RVE, as shown in **Fig. 7.2**. Mathematically it is a minimal volume of the macro-scale one. By definition, RVE, at the same time, has to be substantially large to be statistically representative of the properties, which are regarded as pointwise values of the material system [258].

7.2.1.3. Nano-scale:

The nano-scale system signifies a primary unit cell of those constituting the micro-scale system and defines the material's morphology, such as nanoparticles type, shape, and size. Damage analysis of such a system involves the relationship between the nanostructure and the mechanical behaviour of nanocomposites.

7.2.2. Mean mechanical properties and stiffness tensor

During mechanical loading on the nanocomposite, the stress field ($\hat{\sigma}$) and its corresponding strain field ($\hat{\varepsilon}$) are distributed heterogeneously at a point in the RVE. The average stress (σ) applied at the macro-scale, the corresponding average strain (ε) in the representative average volume V and the analogy between the average nanoparticles stress at the nano-scale (σ_n) and the average nanocomposite stress (σ) is described by [258]. The analysis of dilute composites, which are assumed to avoid unusual particle-particle interactions because of low fibre volume fraction, can be performed by taking advantage of the Dilute Eshelby model. Employing the Mori–Tanaka theorem and the Eshelby global concentration tensors, the link between nano-scale and macroscale can be described shown in Error! Reference source not found.. The radial stress $(\bar{\sigma}_{rr})$ in RVE is equivalent to the applied average stress at macroscopic scale and can be expressed as[257]:

$$\sigma_n = H\sigma = H\bar{\sigma}_{rr} \tag{7.2}$$

Here H denotes the radial component of the stress concentration tensor (SCT) of dilute solution[259]. The selection of RVE type and geometry is crucial and influences the correlations among the nano, micro, and macro scales stress fields. The constitutive relations for this multi-scale modelling involve the local description of the distribution of nanoparticles, interphase and matrix.

7.2.3. Description of RVE

Locally though the nanocomposites are considered non-homogeneous systems, however, sufficiently huge samples at a global scale can be treated based on homogeneous assumptions. A critical objective of the multi-scale modelling of nanocomposite is to derive its dominant properties from its constitutive laws and the local distribution of their constituents. The important consideration is that the proposed RVE must include a large number of the nanocomposite micro-heterogeneity, for example, grains, inclusions, voids, fibres, etc., and simultaneously it must remain small as much as necessary to be regarded as a volume element of continuum mechanics[260]. Among the various possible RVE geometry, the cylindrical RVE with different radii representing the constituent dimensions are found to be more suitable for the analysis of CNT-reinforced nanocomposite and adheres to the true nature of the CNT system[261]. Then the volume elements can be uniformly arranged in a square or hexagonal array to represent the global scale of the composite system. Since the CNT long has a large aspect ratio, a continual cylindrical type representative volume element is justified in the present analysis. In addition, we consider the CNT and RVE to be solid and straight without any curvature.

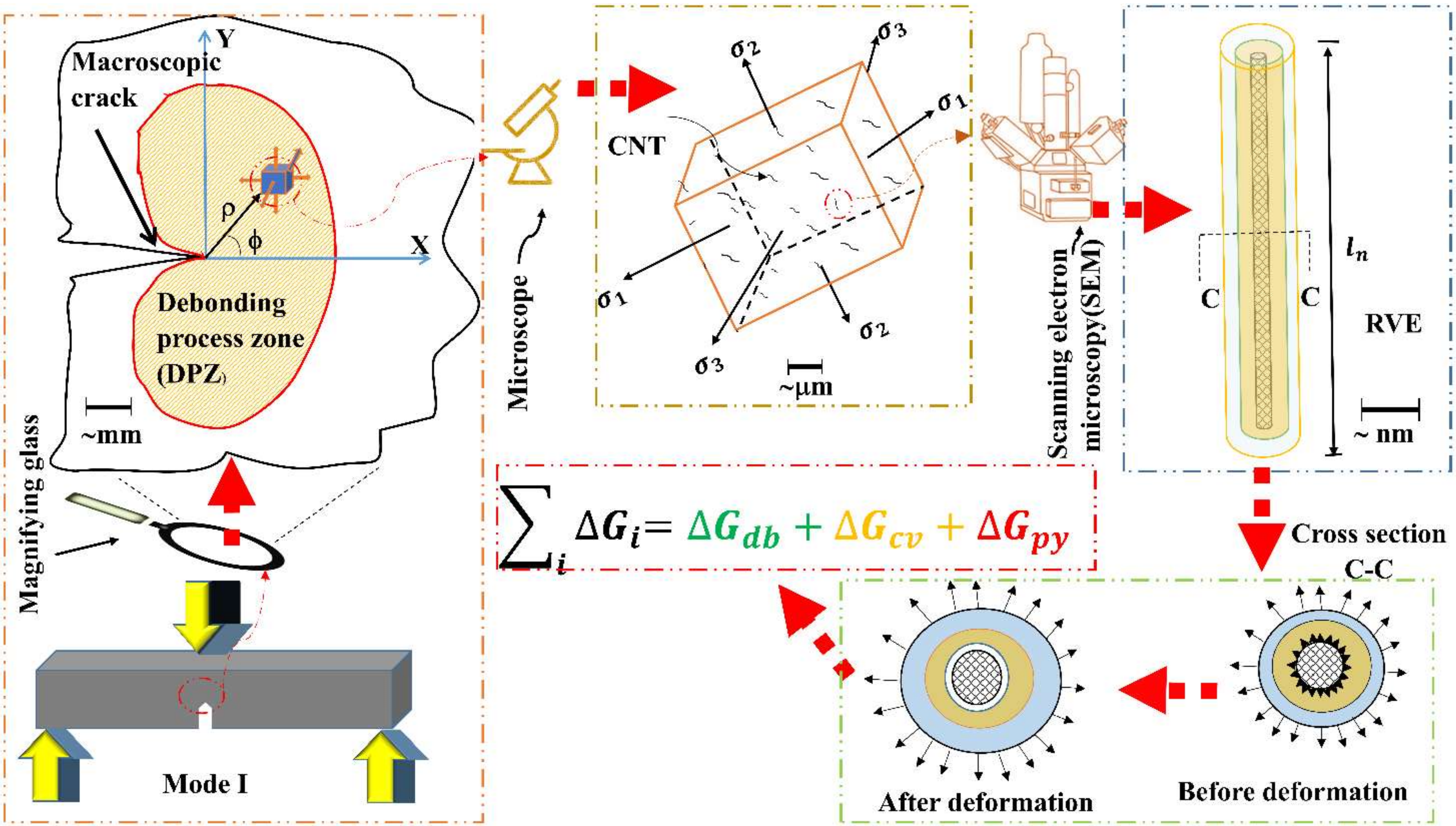

Fig. 7.2. Illustration of multiscale system under analysis.

The interphase characteristics significantly affect the properties and fracture behaviour of the CNT-reinforced nanocomposite. Hence the study of the bond strength of interphase with CNT and resin is crucial to the structural integrity and load-carrying capacity of the material system. The studies on the attachment of the resin molecules with the CNT have affirmed the weak bond between CNT and polymers at the interface[4,262,263]. A weak attachment (interphase) between resins molecules and CNT is also confirmed by Ajayan [264]. Barber [263] reported that the main cause of weak interphase is the uneven dispersion of CNT in resins. Moreover, sometimes nanocomposites exhibit lower mechanical properties than neat resins because of improper and lack of post-cure resins. To estimate the mechanical properties of nanocomposite, which have CNT as reinforcing nanoparticles, Seidel and Shokrieh [265,266] considered the interphase like an identical solid continuum, where the van der Waals interactions have characterized the interphase between neat resin and nanoparticles. In this research, the

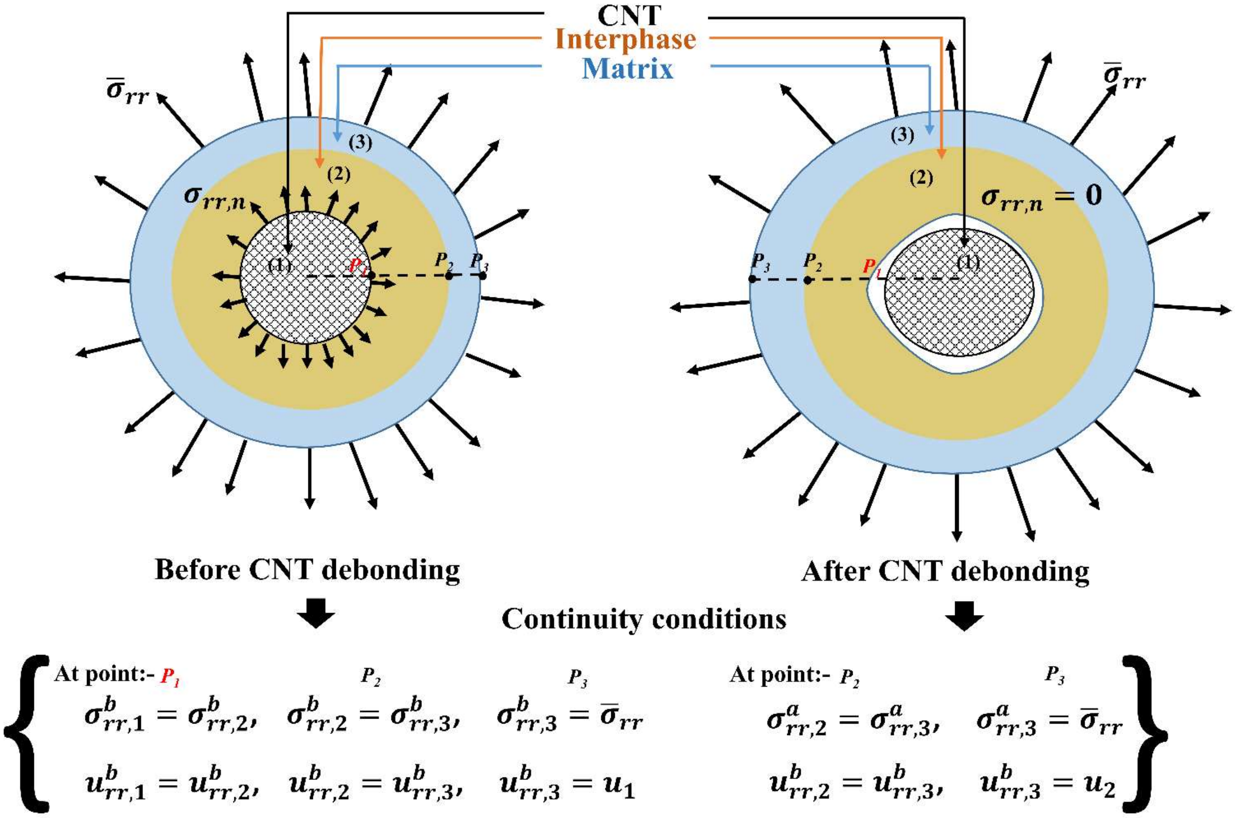

$$\left\{\begin{array}{lllll} \sigma^b_{rr,1} = \sigma^b_{rr,2}, & \sigma^b_{rr,2} = \sigma^b_{rr,3}, & \sigma^b_{rr,3} = \bar{\sigma}_{rr} & \sigma^a_{rr,2} = \sigma^a_{rr,3}, & \sigma^a_{rr,3} = \bar{\sigma}_{rr} \\ u^b_{rr,1} = u^b_{rr,2}, & u^b_{rr,2} = u^b_{rr,3}, & u^b_{rr,3} = u_1 & u^b_{rr,2} = u^b_{rr,3}, & u^b_{rr,3} = u_2 \end{array}\right\}$$

Fig. 7.3. Applied stresses on RVE and continuity conditions before and after debonding.

constituent of RVE is CNT, interphase and neat resin. The cylindrical RVE have CNT in the core, which successively enfolds by the interphase, which was considered a solid continuum phase, and surrounded by neat resin.

7.3.Energy release rate procedure in multi-scale modelling

Assumptions

- The CNT are well bonded to the matrix, and the distribution of CNT into the epoxy must be uniform.
- Each constituent is homogeneous and isotropic, and the agglomeration of CNT must be neglected.
- The fibres are in a hexagonal array, and no contact between the CNT.
- A hydrostatic stress state exists within each constituent of the composite.
- There is no stress interaction between the matrix and neighbouring fibres.
- The diameter and length of created nanovoids after the debonding phenomena have the same as CNT, which afterwards encounters elastic cavitation and plastic deformation.
- All material properties are independent of both the temperature and the moisture.

The crack resistance of nanocomposite is usually analyzed by the processes evolved for homogeneous materials, like the determination of the stress intensity factor or the energy release rate. Energy must be required to propagate an existing crack. To originate crack propagation, the energy release rate, which is available from the change of the elastic energy and the applied loading for an increment of crack growth, must at the least be equal to the energy necessary, known as crack resistance[267,268]. This is a measure of fracture energy. Along the debonding process zone (DPZ), the overall fracture energy of nanocomposites can be expressed as a linear superposition of individual constituent contribution [249,269].

Specifically, the critical strain energy release rate or overall fracture energy (say for Mode I) of nanocomposite is expressed [202,270] as:

$$G_{Ic,nc} = G_{Ic,m} + \sum_i \Delta G_i \tag{7.3}$$

where, $G_{Ic,nc}$ represents critical energy release rate for Mode I fracture of the nanocomposite, $G_{Ic,m}$ and ΔG_i are respectively the fracture energy of pure epoxy or matrix and toughening contribution by the individual mechanism. The later can be stated as

$$\sum_i \Delta G_i = \Delta G_{cd} + \Delta G_{db} + \Delta G_{pull} + \Delta G_{cv} + \Delta G_{SB} + \Delta G_{py} \tag{7.4}$$

All individual energy contributions in Eq. (7.4) are known as; crack deflection(ΔG_{cd}), interfacial debonding(ΔG_{db}), CNTs pull-out (ΔG_{pull}), cavitation(ΔG_{cv}), shear band formation (ΔG_{SB}) and plastic deformation (or yielding) of nanovoids (ΔG_{py}). In the present research, we have focused on interfacial debonding, cavitation and plastic deformation of nanovoids because they are the most dominant modes affecting the criticality of debonding progression. Following the approach to microstructure fracture by Huang [249], empirical relations can be developed to determine ΔG_i and written as

$$\Delta G_i = 2 \int_0^{\rho^*(\phi = \pi/2)} w_i \, d\rho = 2\rho^* w_i \tag{7.5}$$

and

$$w_i = \frac{\Delta U_i}{\mathrm{V}} = \frac{V_f \Delta U_i}{\pi r_n^2 l_n} \tag{7.6}$$

where ρ is DPZ radius while ρ^* also the DPZ radius at angle ϕ with the direction of crack front ($\phi = \pi/2$) (**Fig. 7.2**) and w_i , ΔU_i , V and V_f are the strain energy density, strain energy, total volume of the RVE and volume fraction of CNT in the RVE, respectively. Considering the mean radial stress around RVE (σ_{rr}) responsible for the different toughening mechanisms of the nanocomposite, this can be correlated with the principal stresses in macro-scale fields of nanocomposites as follows:

$$\sigma_{rr} = \frac{\xi_1 \sigma_{11} + \xi_2 \sigma_{22} + \xi_3 \sigma_{33}}{3} \tag{7.7}$$

where ξ_1 ,ξ_2 and ξ_3 are thrice of the square of the cosine of the angles between the axis of principal stresses (σ_{11}, σ_{22} and σ_{33}) and respective radial axis of the cylindrical system. Furthermore,

$$\xi_1 + \xi_2 + \xi_3 = 3 \quad \text{and} \quad 0 \le \xi_1, \xi_2, \xi_3 \le 3 \tag{7.8}$$

Griffith's[271] analysis of fracture was initially intended for homogeneous, isotropic materials. Effective modulus theory allows us to replace the heterogeneous, anisotropic nanocomposite with a corresponding homogeneous, anisotropic substance. It turns out that by considering the stress distribution near the crack tip, we can establish another interpretation of the Griffith analysis that can be used equally well for homogenous isotropic or anisotropic materials, as well as states other than Griffith's simple uniaxial stress. Assuming Hookean behaviour and infinitesimal strains, According to Westergaard[272], specific stress-function solutions connect the local concentration of stresses at the crack tip to the applied stresses. (**Fig. 7.4**) shows the plane strain state near the uniaxially loaded crack tip. In the vicinity of the crack tip, the solutions assume the form.

$$\sigma_{ij} = \sigma \left(\frac{a}{2\rho}\right)^{\frac{1}{2}} f_{ij}(\phi) \tag{7.9}$$

where a is the length of the crack, ρ and ϕ are the point's polar coordinates in the DPZ with the origin at the crack tip, and σ_{ij} is the stress tensor's component at that particular location.

This result was modified by Irwin[273] to:

$$\sigma_{ij} = \frac{K_{I,nc}}{(2\pi\rho)^{\frac{1}{2}}} f_{ij}(\phi) \tag{7.10}$$

where $K_{I,nc}$ is Mode I stress intensity factor of nanocomposite.

Now, the principal stresses in the DPZ at location (ρ, ϕ) can be calculated as:

$$\begin{Bmatrix}\sigma_{11}\\ \sigma_{22}\\ \sigma_{33}\end{Bmatrix} = \begin{Bmatrix}\left(K_{I,nc}/\sqrt{2\pi\rho}\right)\cos\left({}^{\phi}/_{2}\right)\left[1+\sin\left({}^{\phi}/_{2}\right)\right]\\ \left(K_{I,nc}/\sqrt{2\pi\rho}\right)\cos\left({}^{\phi}/_{2}\right)\left[1-\sin\left({}^{\phi}/_{2}\right)\right]\\ v_{nc}(\sigma_{11}+\sigma_{22})\end{Bmatrix} \tag{7.11}$$

where v_{nc} is Poisson's ratio of the nanocomposite. By substituting Eq.(7.11) into Eq.(7.7), the following relation is obtained.

$$\sigma_{rr} = \frac{K_{I,nc}}{3\sqrt{2\pi\rho}}\cos\frac{\emptyset}{2}\times\left\{(\xi_1+\xi_2)+(\xi_1-\xi_2)\sin\left(\frac{\emptyset}{2}\right)+2\,\xi_3 v_{nc}\right\} \tag{7.12}$$

At the macroscale, the effective radial stress ($\bar{\sigma}_{rr}$) distribution in the DPZ can be written as the average of principal stress (σ_{rr}). Thus

$$\bar{\sigma}_{rr} = \frac{1}{\rho}\int_0^{\rho}\sigma_{rr}\,d\rho = \frac{2K_{I,nc}}{3\sqrt{2\pi\rho}}\cos\frac{\emptyset}{2}\times\left\{(\xi_1+\xi_2)+(\xi_1-\xi_2)\sin\left(\frac{\emptyset}{2}\right)+2\,\xi_3 v_{nc}\right\} \tag{7.13}$$

The radial distance from the crack tip can be derived using Eq. (7.13), a function of the angle ϕ.

$$\rho(\emptyset) = \frac{2K_{I,nc}^2}{9\pi\bar{\sigma}_{rr}^2}\cos^2\frac{\emptyset}{2}\times\left\{(\xi_1+\xi_2)+(\xi_1-\xi_2)\sin\left(\frac{\emptyset}{2}\right)+2\,\xi_3 v_{nc}\right\}^2 \tag{7.14}$$

At the crack initiation, stress at nano-scale (σ_n) around the CNT is equal to the critical stress (σ_{cr}), which begins the debonding progression. Now Eq. (7.2) is redefined as:

$$\sigma_{cr} = H\bar{\sigma}_{rr} \tag{7.15}$$

Let's assume that the radial distance of the crack tip in DPZ has a critical value ρ^* at angle $\emptyset = \frac{\pi}{2}$. Now substituting Eq. (7.15) into Eq. (7.14), we get

$$\rho^*\left(\emptyset=\frac{\pi}{2}\right) = \frac{H^2K_{I,nc}^2}{9\pi\sigma_{cr}^2}\times\left\{1.707\xi_1+0.293\,\xi_2+2\,\xi_3 v_{nc}\right\}^2 = \frac{H^2K_{I,nc}^2}{9\pi\sigma_{cr}^2}\times\Psi \tag{7.16}$$

Here, $\Psi = f(\xi_1, \xi_2, \xi_3)$ and it is factored as:

$$\Psi = \left\{1.707\xi_1+0.293\,\xi_2+2\,\xi_3 v_{nc}\right\}^2 \tag{7.17}$$

Let's assume the Poisson's ratio $v_{nc} = 0.33$; now, by applying the mean value theorem for definite triple integral for Eq. (7.17) and (7.8), we found the mean value of the factor $\Psi = 18.757$. Closed for the solution of the fracture energy is known to be

$$G_{Ic,nc} = \frac{K_{I,nc}^2(1-v_{nc}^2)}{E_{nc}}. \tag{7.18}$$

where E_{nc} is the Young's Modulus of the nanocomposite. First solving Eq. (7.5), (7.16) and using Eq. (7.18). we obtained:

$$\Delta G_i = \frac{2H^2 E_{nc}}{9\pi\sigma_{cr}^2} \frac{\Psi}{(1-v_{nc}^2)} w_i G_{Ic,nc} = \Theta w_i G_{Ic,nc} \tag{7.19}$$

where $\Theta = \frac{2H^2 E_{nc}}{9\pi\sigma_{cr}^2} \frac{\Psi}{(1-v_{nc}^2)}$

Eq. (7.19) shows that to estimate each mechanism's fracture energy contribution, the nano-scale displacement fields must be computed.

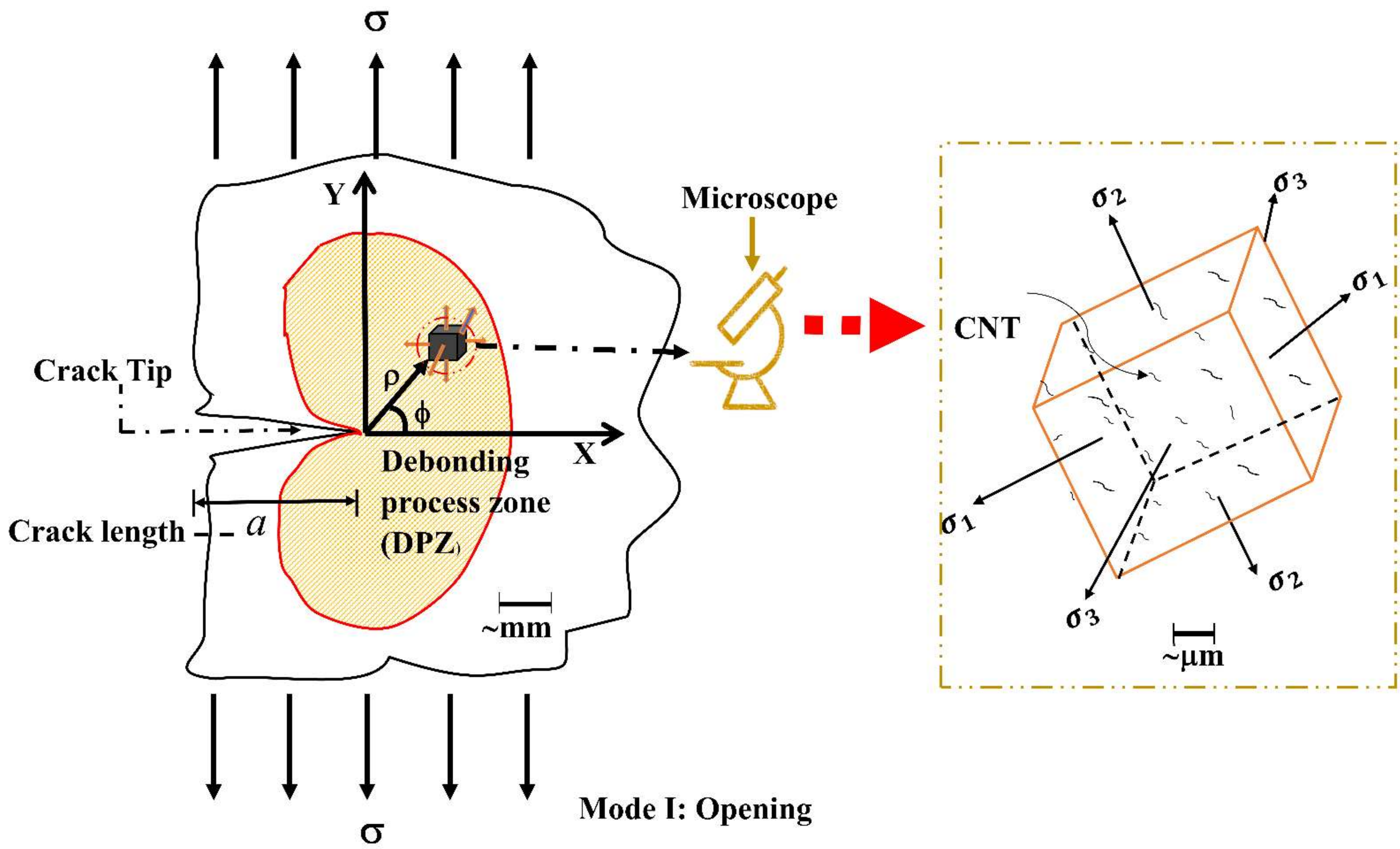

Fig. 7.4 Loading and Stress field near crack tip

7.4.Elastic debonding induced toughness improvement

The presence of CNT in the RVE guarantees a high aspect ratio, so only radial stress is assumed to apply on the lateral surface. The cylindrical symmetry implies that only the radial displacement u is nonzero and independent of the other coordinates θ and z for the RVE[274]. Based on the Cauchy Continuum Theory and presuming the constituents to be isotropic, the equilibrium equation for the axisymmetric cylindrical RVE can be written as:

$$\frac{d\sigma_{rr}}{dr}+\frac{\sigma_{rr}-\sigma_{\theta\theta}}{r}=0 \tag{7.20}$$

$$\frac{d\varepsilon_{rr}}{dr}+\frac{\varepsilon_{\theta\theta}-\varepsilon_{rr}}{r}=0 \tag{7.21}$$

The criticality of debonding process comprises the requires the conditions before and after the debonding of CNT in the RVE. This has been derived in subsequent as:

$$\sigma_{rr,\Omega}=B_{\Omega}+\frac{A_{\Omega}}{r^2} \tag{7.22}$$

$$u_{rr,\Omega}=\frac{v_{\Omega}}{\lambda_{\Omega}}B_{\Omega}r-\frac{A_{\Omega}}{2\mu_{\Omega}r} \tag{7.23}$$

where $(\lambda_{\Omega},\mu_{\Omega})$ and (B_{Ω},A_{Ω}) are the Lame constants and coefficients of respective Ω^{th}sub-domain, with Ω = *n, i, m*, where *n, i, m* are the notations meant for the CNT (*n*), the interphase (*i*) and the matrix (*m*), respectively. The debonding process's criticality comprises the requirements before and after CNT's debonding in the RVE. Lame constants before CNT debonding (Condition for debonding initiation) have been derived by [72]:

$$A_m^b=\xi_b\sigma_{cr} \quad \text{and} \quad B_m^b=\zeta_b\sigma_{cr} \tag{7.24}$$

where the ξ_b and ζ_b are defined in *Supplementary*. The radial displacement distribution in the matrix sub-domain can be rewritten as[72]:

$$u_1=u_{rr,m}^b=\left\{\frac{v_m}{\lambda_m}r_m\zeta_b-\frac{\xi_b}{2u_m r_m}\right\}\sigma_{cr} \text{ and } H=\frac{1}{\zeta_b+\frac{\xi_b}{r_m^2}} \tag{7.25}$$

Now, after CNT debonding (Condition for successive debonding progression), the radial distribution of stress and displacement in the RVE for the Ω^{th}sub-domain are derived as follow[72]:

$$A_m^a = \xi_a \sigma_{cr} \quad \text{and} \quad B_m^a = \zeta_a \sigma_{cr} \tag{7.26}$$

The superscript "a" is noted after CNT debonding condition. The displacement in the matrix sub-domain is also derived [72] as:

$$u_2 = u_{rr,m}^a = \left\{ \frac{v_m}{\lambda_m} r_m \zeta_a - \frac{\xi_a}{2u_m r_m} \right\} \sigma_{cr} \tag{7.27}$$

The dissipated energy also contributing to the toughening of the nanocomposites during the debonding phenomena of CNT is known as strain energy. The strain energy during the debonding phenomena of CNT is defined as[274]:

$$\Delta U_{db} = \frac{1}{2} P(u_2 - u_1) = \frac{1}{2} P\left(u_{rr,m}^a - u_{rr,m}^b\right) \tag{7.28}$$

where P is the applied load at the outer lateral area of RVE, i.e., matrix phase for the cylindrical geometry, is defined as:

$$P = 2\pi r_m l_n \bar{\sigma}_{rr} \tag{7.29}$$

where l_n is denoted length of CNT.

The strain energy dissipated during the debonding mechanism creates a new lateral area around the CNT. The newly developed lateral area is equal to CNT ($2\pi r_n l_n$). Then the interface fracture or adhesive energy[275,276] of the CNT debonding γ_i is related as[274]:

$$\Delta U_{db} = 2\pi r_n l_n \gamma_i \tag{7.30}$$

Now the interface fracture calculated from Eq. (7.30) as:

$$\gamma_i = \frac{\Delta U_{db}}{2\pi r_n l_n} \tag{7.31}$$

The strain energy density due to the fracture energy contribution in toughening of nanocomposite through debonding can be defined as:

$$w_{db} = \frac{V_f \Delta U_{db}}{\pi r_n^2 l_n} \tag{7.32}$$

Substituting Eq. (7.32) to Eq. (7.19), the toughness improvement due to the CNT debonding is evaluated to be:

$$\Delta G_{db} = \Theta\, w_{db} G_{Ic,nc} \tag{7.33}$$

7.5.Cavitation

After debonding CNT, cavitation (in **Fig. 7.3**) occurs in the nanocomposite, which prefers to grow around the CNT in the interphase region. It is noted that the improvement of fracture toughness due to cavitation is more significant for rod nanoparticles than spherical and sheet nanoparticles. An instant after debonding, the stress at the CNT vanishes to zero $\sigma_{rr,i}^{a}\,|_{r=r_n} = 0$ due to the creation of the cavity between interphase and CNT. Let's assume the radius of the cavity is r_c and the displacement of CNT surface being $u_{rr,c}^{a}$. Then the volume of the cavity ($\pi r_c^2 l_n$) is equal to the product of lateral surface area of CNT multiplied by the displacement of the CNT surface $u_{rr,c}^{a}$. Hence

$$\pi r_c^2 l_n = 2\pi r_n l_n u_{rr,c}^{a} \tag{7.34}$$

From the above Equation, we can evaluate the radius of the cavity created i.e.

$$r_c = \sqrt{2 r_n u_{rr,c}^{a}} \tag{7.35}$$

Now, we go through Eq. (7.22) and (7.23), again we know $\sigma_{rr,n}^{a}\,|_{r=r_n} = 0$, after debonding of CNT and using the continuity conditions i.e.,**Fig. 7.3**;

$$\begin{aligned} &\sigma_{rr,n}^{a}\,|_{r=r_n} = 0, \qquad u_{rr,i}^{a}\,|_{r=r_n} = u_{rr,c}^{a} \\ &\sigma_{rr,i}^{a}\,|_{r=r_i} = \sigma_{rr,m}^{a}\,|_{r=r_i}, \qquad \sigma_{rr,m}^{a}\,|_{r=r_m} = \bar{\sigma}_{rr}, \qquad u_{rr,i}^{a}\,|_{r=r_i} \\ &\qquad = u_{rr,m}^{a}\,|_{r=r_i}. \end{aligned} \tag{7.36}$$

We derived the following expression for the displacement:

$$u_{rr,i}^{a}\,|_{r=r_n} = u_{rr,c}^{a} = \left(\zeta_a + \frac{\xi_a}{r_i^2}\right)\frac{r_i^2 r_n}{r_i^2 - r_n^2}\left\{\frac{v_i}{\lambda_i} + \frac{1}{2u_i}\right\}\sigma_{cr} \tag{7.37}$$

where ξ_a and ζ_a are expressed in *Supplementary*. Here energy dissipated to create a cavity around CNT is written as:

$$\Delta U_{cv} = \pi r_n l_n u_c^a \sigma_{cr} \tag{7.38}$$

The strain energy density due to cavitation is defined as:

$$w_{cv} = \frac{V_f \Delta U_{cv}}{\pi r_n^2 l_n} \tag{7.39}$$

And the toughness improvement due to cavitation becomes:

$$\Delta G_{cv} = \Theta\, w_{cv} G_{Ic,nc} \tag{7.40}$$

7.6.Plastic deformation of nanovoids

The cohesive energy (or surface energy) of the CNT has a crucial effect on the improvement of fracture toughness of nanocomposite. The energy governs the elastic debonding and cavitation condition. This mechanism stimulates the growth of nanovoids around the CNT, which retains the same dimension as CNT. Still, the local yielding of the nanovoids is initiated by the local stress field, which is enough for it around the CNT. However, the plastic properties of the interphase and matrix regulate the growth of the nanovoids. Let's assume r_p as the radius of the extended plastic zone within the RVE. There are two different possibilities, which are defined as:

1. $r_p < r_i$, Means yielding occurred only in the interphase zone.
2. $r_i < r_p < r_m$, Means yielding occurred in the whole interphase region and partially in the matrix.

Pertinent literature studies have reported evidence about the elastic-plastic response of the matrix and the interphase where the materials were seen to obey power-law hardening[274,277–279]. Till the yield limit, the hardening behaviour can be preserved as an elastic response and subsequently, in the plastic region, a power law for the stresses and strains is stated.

$$\begin{cases} \bar{\varepsilon}_P = \dfrac{\bar{\sigma}_P}{E} & if\ \ \bar{\sigma}_P \leq \sigma_Y \\ \dfrac{\bar{\varepsilon}_P}{\varepsilon_Y} = \left(\dfrac{\bar{\sigma}_P}{\sigma_Y}\right)^n & if\ \ \bar{\sigma}_P \geq \sigma_Y \end{cases} \tag{7.41}$$

Here $\varepsilon_Y = \frac{\sigma_Y}{E}$, while $\bar{\sigma}_P$, $\bar{\varepsilon}_P$ and n are the equivalent plastic stress, strain and hardening exponents of material, respectively.

Invoking the well-known Tresca criterion, the equivalent plastic stress can be estimated as:

$$\sigma_{\theta\theta} - \sigma_{rr} = 2\bar{\sigma}_P \tag{7.42}$$

The deviatoric stress and hydrostatic stress (or mean pressure) component of the plastic stress tensor are related:

$$S_{ij}^{p} = \sigma_{ij} - \frac{1}{3}\sigma_{kk}\delta_{ij} \tag{7.43}$$

Here $(i, j = r, \theta, z)$ are the cylindrical axis of the RVE, and the superscript represents the plastic state. S_{ij}^{p} is the deviatoric stress component of the plastic stress tensor, and the plastic stress tensor also has the hydrostatic stress component, which is defined as $\sigma_{kk} = \frac{\sigma_{rr}+\sigma_{\theta\theta}+\sigma_{zz}}{3}$. While δ_{ij} is Kronecker symbol defined as:

$$\delta_{ij} = \begin{cases} 1 & when\ i = j \\ 0 & when\ i \neq j \end{cases} \tag{7.44}$$

Three conditions, closed-end, open-end and plane strain, arise for solving the problem in the cylindrical coordinate system. For simplicity and a closed-form solution, we consider closed-end conditions for the RVE. For the closed-end condition, σ_z is precisely the mean of the other two principal stresses[277,278,280]. Now Eq. (7.23) can be redefined as:

$$S_{ij}^{p} = \sigma_{ij} - \frac{\sigma_{rr}+\sigma_{\theta\theta}}{2} \tag{7.45}$$

The relationship between the plastic components of the strains to the stresses is proposed with Hencky's stress-strain relation [280] stated as follows

$$\varepsilon_{ij}^{p} = \lambda_p S_{ij}^{p} \tag{7.46}$$

where λ_p is positive and zero during loading and unloading, respectively and depends on the equivalent stress $\bar{\sigma}_P$. Its value is derived by von Mises yield criterion and Hencky's stress-strain relation[280]. Then Eq. (7.46) is redefined as:

$$\varepsilon_{ij}^{p} = \frac{3}{2}\frac{\bar{\varepsilon}_P}{\bar{\sigma}_P} S_{ij}^{p} \tag{7.47}$$

Utilizing Eq. (7.41), the above Eq. (7.47) can be written as:

$$\varepsilon_{ij}^{p} = \frac{3}{2}\frac{\varepsilon_Y}{\sigma_Y}\left(\frac{\bar{\sigma}_P}{\sigma_Y}\right)^{n-1} S_{ij}^{p} \tag{7.48}$$

We can derive the following relation using Eq. (7.36) and (7.39).

$$S_{rr}^{p} = -\bar{\sigma}_P \qquad \text{and} \qquad S_{\theta\theta}^{p} = \bar{\sigma}_P \tag{7.49}$$

With the help of Eq. (7.48) and (7.49), the plastic strain can be determined as:

$$\varepsilon_{rr}^{p} = -\frac{3}{2}\varepsilon_Y\left(\frac{\bar{\sigma}_P}{\sigma_Y}\right)^{n} \tag{7.50}$$

and

$$\varepsilon_{\theta\theta}^{p} = \frac{3}{2}\varepsilon_Y\left(\frac{\bar{\sigma}_P}{\sigma_Y}\right)^{n} \tag{7.51}$$

Substituting Eq. (7.50) and (7.51) into the compatibility equation, Eq. (7.20) and (7.21), then:

$$n\frac{\partial\bar{\sigma}_P}{\partial r} + 2\frac{\bar{\sigma}_P}{r} = 0 \tag{7.52}$$

The general solution of the partial differential equation, Eq. (7.52), is given as:

$$\bar{\sigma}_P = Cr^{-\frac{2}{n}} \tag{7.53}$$

The plastic radial stress σ_{rr}^{p}, is derived by substitution of Eq. (7.53) and (7.42) into Eq. (7.20) and found as:

$$\sigma_{rr}^{p} = D - nCr^{-\frac{2}{n}} \tag{7.54}$$

Then in the plastic region, the absolute solution for the radial distribution of stress and displacement is:

$$\bar{\sigma}_{P,\Omega} = C_\Omega r^{-\frac{2}{n_\Omega}} \tag{7.55}$$

$$\sigma_{rr}^{p} = D_{\Omega} - n_{\Omega} C_{\Omega} r^{-\frac{2}{n_{\Omega}}} \tag{7.56}$$

$$u_{rr,\Omega}^{p} = \varepsilon_{rr,\Omega}^{p} r = -\frac{3}{2}\varepsilon_{Y,\Omega}\left(\frac{\bar{\sigma}_{P,\Omega}}{\sigma_{Y,\Omega}}\right)^{n_{\Omega}} r = -\frac{3}{2}\frac{\varepsilon_{Y,\Omega}}{r}\left(\frac{C_{\Omega}}{\sigma_{Y,\Omega}}\right)^{n_{\Omega}} \; with\,\Omega$$

$$= \begin{cases} i \;\; when \;\; r_p < r_i \,, \\ m \;\; when \;\; r_i < r_p < r_m \end{cases} \tag{7.57}$$

The stress and displacement fields outside the plastic region within the Ω^{th} sub-domain is defined as:

$$\sigma_{\theta\theta,\Omega}^{*} = B_{\Omega}^{*} - \frac{A_{\Omega}^{*}}{r^2} \tag{7.58}$$

$$\sigma_{rr,\Omega}^{*} = B_{\Omega}^{*} + \frac{A_{\Omega}^{*}}{r^2} \tag{7.59}$$

$$u_{rr,\Omega}^{*} = \frac{v_{\Omega}}{\lambda_{\Omega}} B_{\Omega}^{*} r - \frac{A_{\Omega}^{*}}{2\mu_{\Omega} r} \tag{7.60}$$

Here star ($*$) represent the elastic region. The continuity conditions are applied between the interphase and matrix and at the boundary where the elastic region transforms into plastic region. The continuity conditions (as **Fig. 7.3**) denoted in notation form for plastic deformation as below and applied to Eq. (7.55) to (7.55,

$$\sigma_{rr,i}^{p}\big|_{r=r_n} = 0,\; \sigma_{rr,i}^{p}\big|_{r=r_i} = \sigma_{rr,m}^{p}\big|_{r=r_i},\; \sigma_{rr,m}^{*}\big|_{r=r_m} = \bar{\sigma}_{rr}\,,\; \bar{\sigma}_{P,\Omega}\big|_{r=r_p} = \sigma_{Y,m},$$
$$u_{rr,i}^{p}\big|_{r=r_i} = u_{rr,m}^{p}\big|_{r=r_i},\;\; \sigma_{\theta\theta,m}^{*}\big|_{r=r_p} - \sigma_{rr,m}^{*}\big|_{r=r_p} = \sigma_{Y,m},\; \sigma_{rr,m}^{p}\big|_{r=r_p} = \sigma_{rr,m}^{*}\big|_{r=r_p} \tag{7.61}$$

We found the constant, i.e., the solution of the previous system is:

$$C_i = \sigma_{Y,i}\left(\frac{\varepsilon_{Y,m}}{\varepsilon_{Y,i}}\right)^{\frac{1}{n_i}} \left(r_p\right)^{\frac{2}{n_i}} \quad and \qquad D_i = n_i \sigma_{Y,i}\left(\frac{\varepsilon_{Y,m}}{\varepsilon_{Y,i}}\right)^{\frac{1}{n_i}} \left(\frac{r_p}{r_i}\right)^{\frac{2}{n_i}}, \tag{7.62}$$

$$C_m = \sigma_{Y,m}\left(r_p\right)^{\frac{2}{n_m}} \; and \quad D_m = \left\{ n_i \sigma_{Y,i} \left(\frac{\varepsilon_{Y,m}}{\varepsilon_{Y,i}}\right)^{\frac{1}{n_i}} \left(\frac{r_p}{r_i}\right)^{\frac{2}{n_i}} \left[\left(\frac{r_i}{r_n}\right)^{\frac{2}{n_i}} - 1\right] + n_m \sigma_{Y,m} \left(\frac{r_p}{r_i}\right)^{\frac{2}{n_m}} \right\} \tag{7.63}$$

$$A_m^* = -\sigma_{Y,m} r_p^2 \qquad and \qquad B_m^* = \bar{\sigma}_{rr} + \frac{\sigma_{Y,m} r_p^2}{r_m^2} \cong \frac{\sigma_{cr}}{H} \tag{7.64}$$

Now, substituting the above-derived constants, i.e., Eq (7.62) (7.63) and (7.64) into the last boundary condition of Eq. (7.61) and solving those complicated equations then, we figured out the following Equation :

$$\bar{\sigma}_{rr} - \sigma_{Y,m}(1 - n_m) = \left\{ n_i \sigma_{Y,i} \left(\frac{\varepsilon_{Y,m}}{\varepsilon_{Y,i}}\right)^{\frac{1}{n_i}} \left(\frac{r_p}{r_i}\right)^{\frac{2}{n_i}} \left[\left(\frac{r_i}{r_n}\right)^{\frac{2}{n_i}} - 1\right] + n_m \sigma_{Y,m} \left(\frac{r_p}{r_i}\right)^{\frac{2}{n_m}} \right\} \tag{7.65}$$

The above Eq. (7.65) can be solved numerically to obtain the plastic zone radius. Alternately, assuming $n_m \approx n_i$ We can derive the approximate value of the r_p as:

$$r_p \approx r_i \left\{ \frac{\frac{\sigma_{cr}}{H\sigma_{\mathrm{Y},m}} - (1 - n_m)}{n_m \frac{\sigma_{\mathrm{Y},i}}{\sigma_{\mathrm{Y},m}} \left(\frac{\varepsilon_{\mathrm{Y},m}}{\varepsilon_{\mathrm{Y},i}}\right)^{\frac{1}{n_m}} \left[\left(\frac{r_i}{r_n}\right)^{\frac{1}{n_m}} - 1\right] + n_m} \right\}^{\frac{n_m}{2}} \tag{7.66}$$

Using Eq. (7.62), (7.66) and (7.60), we can find the displacement at $r = r_p$ in yielded state as:

$$u_{rr,m}^* = \frac{v_m}{\lambda_m} r_m B_m^* - \frac{A_m^*}{2u_m r_m} \tag{7.67}$$

Finally, the difference between the displacement of the un-yielded state and yielded state is defined as:

$$\Delta u_p = u_{rr,m}^* - u_{rr,m}^a \tag{7.68}$$

Here $u_{rr,m}^a$ is already defined in Eq. (7.27).

Now energy dissipated during yielding can be derived as:

$$\Delta U_{py} = P\Delta u_p = 2\pi r_m l_n \bar{\sigma}_{rr}\left(u_{rr,m}^* - u_{rr,m}^a\right) \tag{7.69}$$

The strain energy density due to strain hardening behaviour for the interphase and the matrix can be evaluated as

$$w_{py} = \frac{V_f \Delta U_{py}}{\pi r_n^2 l_n} \tag{7.70}$$

and also the toughness improvement due to this is determined as:

$$\Delta G_{py} = \Theta\, w_{py} G_{Ic,nc} \tag{7.71}$$

7.7.Results and discussion

To effectively interpolate the developed model to nanocomposites, the mechanical properties of nanocomposites, particularly the fracture toughness, might distinctly depend on the morphology of constituent nanoparticles. This is governed by various characteristics such as the chemical nature of the ingredient, the synthesis procedures employed etc. Unluckily, as far as the researchers are familiar, in the mathematical modelling of the nanocomposite, there are no proper relationships that correlate the synthesis factors and chemical properties of ingredients to the morphology of nanoparticles. Likewise, in the present model, which has been introduced for fracture toughness enhancement at the nano-scale instigated by interfacial debonding, cavitation and plastic deformation of nanovoids, the effect of morphology (as waviness, spiral structure etc.) of CNT is not considered. It has also been presumed that the agglomeration is negligible and dispersion of CNTs within the volume is uniform. All the geometry and material parameters used in the present study and the comparative results obtained using the current approach are mentioned in Error! Reference source not found.. Here, t he dominance of key variable criteria on normalized critical debonding stress and fracture toughness enhancement is explored by employing the available data. The thickness, Young's modulus, yield strength, stress hardening index of interphase and weight fraction of CNT are the dominant criteria for fracture control. A comparison of the estimated fracture toughness in the present model with experimental results and analytical data is summarised in **Table 7.2.**

7.7.1. Effect of the interphase properties on cavitation-induced toughness improvement

The progressive debonding and subsequent formation of cavitation around the nanoparticle and interphase interface triggers the formation of a void, enhancing the fracture resistance. This nano effect might be ascribed to the considerable plastic strain induced with further loading[72,281] . Here two different sets of numerical examples are performed to understand the influence of interphase thickness and stiffness on fracture characteristics with strain energy release rate as the defining parameter. For one set, thickness t has been kept constant at 5 nm and λ is varied from 1 to 6, while for the other set λ it is assumed to be 2 with t varying from 2 nm to 12 nm. The general observation is that with the CNT weight fraction increased from 0.1% to 1%, there has been a steady increase of toughness, and towards the end, the increase is abrupt, as displayed in **Fig. 7.5(a & b)**. But,at the stiffness ratio $\lambda = 2$**,** results distinctly suggest that the increase of the interphase thickness offers a reduced improvement of fracture (Error! Reference source not found. **a**) and for the interphase thickness $t = 5$ nm, with the increase of the stiffness of interphase compared to matrix fracture toughness, decreases, though for both the cases the patterns and distribution are similar. This can be predicted that reducing the interphase stiffness is more effective in toughness enhancement than thickness reduction due to the significant rise in the slope of energy release rate plots in the former case. However, there might be an opinion that both parameters are different, one being geometric and the other material property, to conclusively give any evidence to the observation.

The origination of debonding is the root of other energy dissipation mechanisms as the yielding of the nanovoids, which are created during debonding and cavitation. The yielding of nanovoids is discussed in the next section.

7.7.2. Growth of nanovoid and plastic deformation

The growth of nanovoid and plastic deformation, as discussed in earlier sections and the energy release rate derivations surmises the important mechanism for enhancing energy release rate.

For further evidence, the hardening exponent (*n*), interphase thickness (*t*) and stiffness ratio (λ) are varied sequentially, keeping the other two parameters' constants. For nanocomposites, the nanovoids distribution and the energy absorbed during the yielding of these nanovoids are essential for fracture toughness improvement. Softer interphases contribute to the excessive number of nanovoids, while stiffer interphase is responsible for fewer nanovoids. **Fig. 7.6 (a, b & c)** has underlined that the fracture energy enhancement because of plastic deformation of nanovoids is mainly dependent on the mechanical properties of interphase as well as the thickness of the interphase. The yield strength of interphase($\sigma_{\mathrm{Y},i} = 75\ \mathrm{MPa}$) and matrix ($\sigma_{\mathrm{Y},m} = 68\ \mathrm{MPa}$) are considered from the available literature [281], and the hardening exponents of epoxy, as mentioned [282], are taken from a range of 1 to 13. The following three conditions are analyzed for determining strain energy release rate parameters. Variation of the hardening exponent (*n*), interphase thickness (*t*) and stiffness ratio (λ):

(a) $n = 5$ and $t = 5$ nm and $\lambda = 1, 2, 4, 6$

(b) $\lambda = 2$ and $t = 5$ nm and $n = 1, 3, 5, 6$

(c) $\lambda = 2$ and $n = 5$ and $t = 2$ nm, 5 nm, 8 nm, 12 nm

From **Fig. 7.6**, it can be concluded that fracture energy enhancement due to the plastic deformation of nanovoids increases with increasing the interphase thickness and stiffness, as well as the hardening exponent for all three described cases. Though with an increase of stiffness and thickness (**Fig. 7.6 a** and **c**), the energy release rate values are higher, with hardening exponent, the growth rate (**Fig. 7.6 b**) is rapidly indicated by the gradients of the plots. The hardening exponent is a known key parameter for the plastic deformation of nanovoids. In comparison to earlier energy plots of debonding and cavitation, this explains the evidence that during the plastic deformation of nanovoids, energy absorption is higher than the other mechanism. Therefore, it can be summarized that, unlike debonding and cavitation mechanisms, the plastic deformation of nanovoids is the cardinal mechanism for fracture toughness improvement.

7.7.3. Experimental comparison of fracture energy, analytical evaluation and error

Invoking Eq. (7.3) for the occasional damaging mechanism ΔG_i, the thorough fracture toughness of nanocomposite can be determined. Thereby, by substituting Eq. (7.33) ,(7.40) and (7.71) into Eq. (7.3), we get the overall fracture energy of the nanocomposite as a function of $G_{Ic,m}$ and V_f

$$G_{Ic,nc} = \frac{G_{Ic,m}}{1 - V_f \Theta(\Delta U_{db} + \Delta U_{cv} + \Delta U_{py})} \tag{7.72}$$

The theoretical estimations of fracture energy of the nanocomposite obtained by the above Equation and the results reported in [70,117] with the available material data are put into contrast for validation. Though the present work's analytical assumption and damage mechanism description may not have a one-to-one correspondence or correlation, a qualitative inference is carried out. Error percentage is evaluated with respect to experimental values of fracture energy $G_{Ic,nc}$. The results of the present model and the comparative values of fracture energy are listed in Error! Reference source not found.. It does appear that in some cases the a uthors distinctly provide in the original research all the parameters compulsory to the investigation, while in other cases, some parameters have been presumed by analogy with similar systems. It is manifested that for a low CNT weight fraction percentage (less than 0.5%), the agreement seems adequate. However, the experimental values are reserved at a higher weight fraction (0.5%), indicating an error percentage of 37.51%. There might be a possibility of whether it is an uneven distribution of nanoparticles or any other experimental uncertainty, or any other damage mechanism influencing the prescribed verification. The tendency of CNT particles to agglomerate beyond a particular value of weight fraction percentage observed experimentally might contradict the presumption of uniform distribution and dispersion considered in this work.

Significantly, for MWCNT cases, at a higher weight percentage (= 1%), the error percentage is considerably less (6.79%) compared with experimentation, and errors escalate at 0.1% and 0.5%. However, the present result matches well with other analytical models. However, it can be ascertained renovate the competence of the model. Further, the influence of the other toughness mechanisms taking place at the DPZ, such as the crack deflection and shear band formation, must be considered as well as the current mechanisms. However, this might further complicate addressing the individual damage mechanism models bringing into non-negotiable interactions and assumptions having limited effect on fracture toughness enhancement.

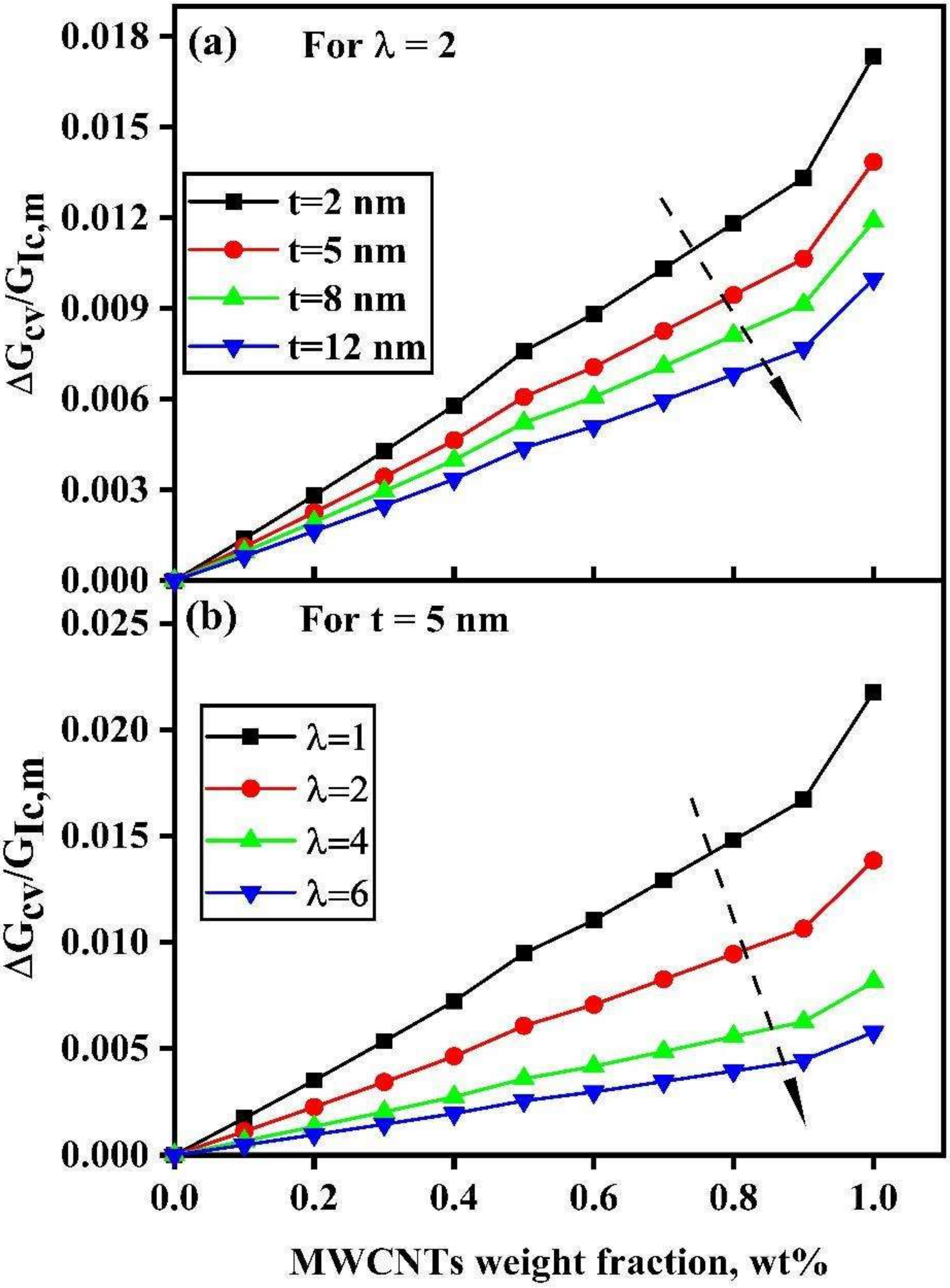

Fig. 7.5. Normalized energy release rate enhancement due to cavitation; considering different (a) interphase thicknesses (t) and (b) interphase stiffness($E_i = \lambda E_m$).

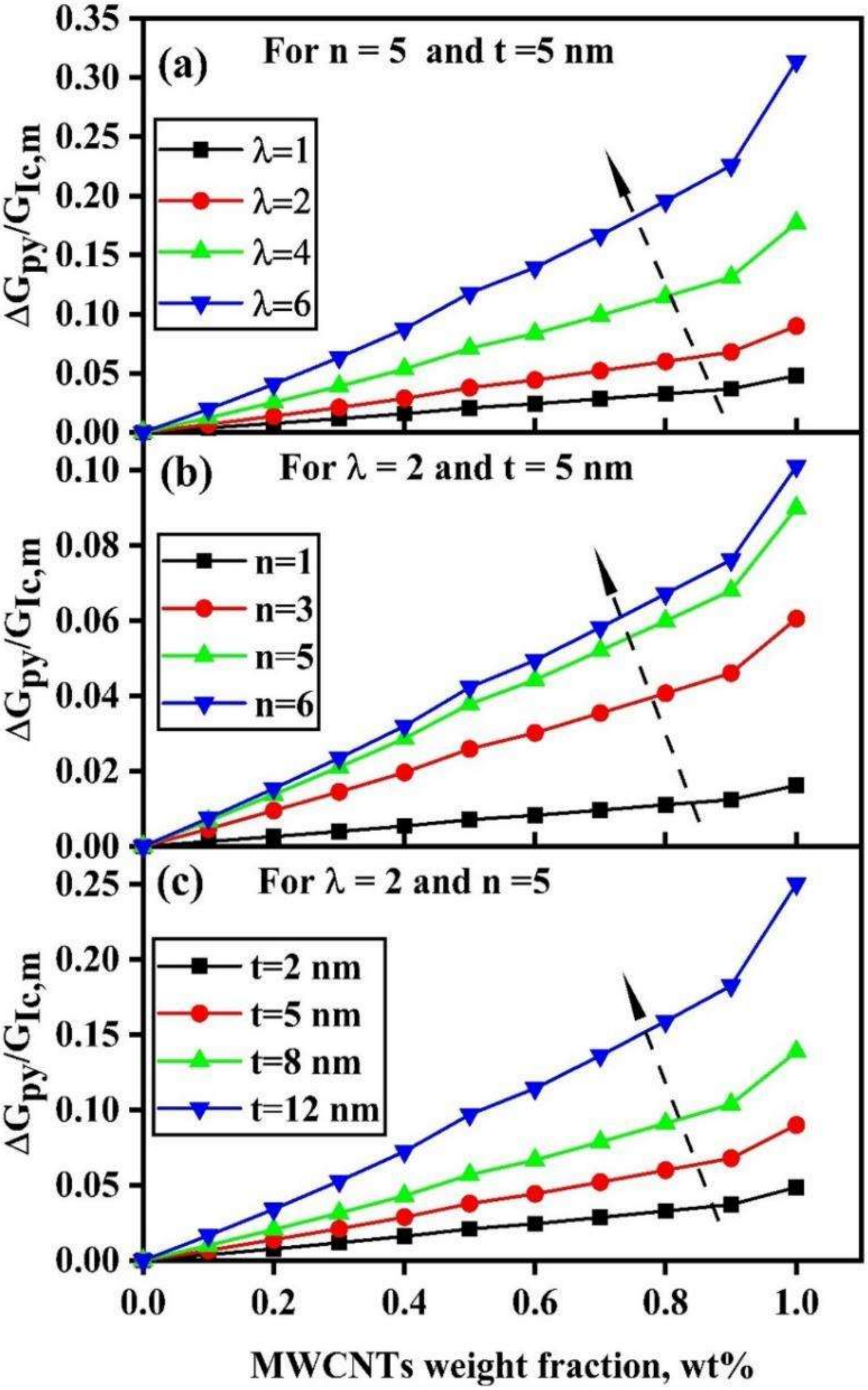

Fig. 7.6. Normalized energy release rate enhancement due to plastic deformation of nanovoids; considering different (a) interphase stiffness($E_i = \lambda E_m$), (b) hardening exponents (n) and (c) interphase thicknesses (t).

Table 7.1. Summary of all parameters used in the present study

Ref.	**CNT**	**r_n (nm)**	**l_n (μm)**	**E_n (TPa)**	**E_m (GPa)**	**γ_i (J/m^2)**	**$\sigma_{y,i}$ (MPa)**	**$\sigma_{y,m}$ (MPa)**
[117]	CNT	60	120	1.1	2.90	25	75[a]	68[a]
[70]	MWCNT	7.50	20	1.1	3.15	0.170	75[a]	68[a]

[a] **The experimentally determined values from Chen J Kang** [281].

Table 7.2. Comparison of the present study results with experimental and analytical predictions found in the literature

Ref.	**CNT**	**Wt%**	**V_f%**	**E_{nc}(GPa)**	**$G_{Ic,nc}$ (J/m^2)**				**Error (%)**
					Present Model	Exp.	Analyt.	Analyt	
[117]	CNT	0	0	2.90	--	133	--	--	
		0.1	0.0534	3.01	138.53	162	159	145[a]	14.5
		0.2	0.1068	3.11	148.52	188	184	162[a]	21.00
		0.5	0.2674	3.26	306.64	223	213	189[a]	37.51
[70]	MWCNT	0	0	3.15	--	742.4	--	--	
		0.1	0.0534	3.24	749.16	951.5	743.20[b]	--	21.30
		0.5	0.1603	3.51	782.04	1056.5	746.90[b]	--	26.00
		1	0.2674	3.69	838.55	899.5	752.00[b]	--	6.79

[a and b] **The analytically determined values from Hamedi** [283] **and Shokrieh MM**[72]**, respectively.**

7.8. Conclusions

A strain energy release rate procedure based on multi-scale and multi-mechanism techniques is developed in this work to investigate the fracture characteristics of CNT/epoxy nanocomposites. The radial distribution of stress at the macro, micro, and nano-scale has been estimated to forecast the fracture toughness improvement due to the origination of CNT interphase debonding, cavitation and plastic deformation of nanovoids along the interface. The cavitation and the mechanism of plastic deformation of the nanovoids are shown to be very much affected by the weight fraction of nanotubes, interphase thickness, moduli ratio of interphase and epoxy matrix and the exponent of plasticity. The fracture energy estimation matches well with available experimental and analytical results at a low weight fraction of less than 0.5% of nano inclusion. The performance of the present model is encouraging, as revealed by the qualitative agreement of the current model with similar experimental and analytical data collected from the literature.

Supplementary

Calculation of coefficients A_m^b, B_m^b, A_m^a and B_m^a

The sobriety of the displacement singularity and finite stress distribution in the CNT suggests that these circumstances are possible if and only if the coefficient A_n^b is equal to zero. Hence applying the continuity conditions i.e., **Fig. 7.3**,

$$\sigma_{rr,n}^b\big|_{r=r_n} = \sigma_{cr} = \sigma_{rr,i}^b\big|_{r=r_n}, \tag{7.73}$$

Applying in the Eq. (7.22) and (7.23);

$$\sigma_{cr} = B_n^b = B_i^b + \frac{A_i^b}{r_n^2} \quad \text{and} \quad u_{rr,n}^b = \frac{v_n}{\lambda_n} B_n^b r_n \quad \text{or} \quad u_{rr,n}^b = \frac{v_n}{\lambda_n} r_n \sigma_{cr} \tag{7.74}$$

Again, the continuity condition (**Fig. 7.3**) is as follows:

$$\sigma_{rr,i}^b\big|_{r=r_i} = \sigma_{rr,m}^b\big|_{r=r_i} \tag{7.75}$$

Applying the Eq. (7.22)

$$B_i^b + \frac{A_i^b}{r_i^2} = B_m^b + \frac{A_m^b}{r_i^2} \tag{7.76}$$

Further by continuity conditions as;

$$u_{rr,n}^b\big|_{r=r_n} = u_{rr,i}^b\big|_{r=r_n} = u_{rr,i}^b\big|_{r=r_i} = u_{rr,m}^b\big|_{r=r_i} \tag{7.77}$$

Applying in the Eq. (7.23);

$$\begin{aligned} u_{rr,n}^b &= \frac{v_i}{\lambda_i} B_i^b r_n - \frac{A_i^b}{2\mu_i r_n} = \frac{v_i}{\lambda_i} B_i^b r_i - \frac{A_i^b}{2\mu_i r_i} = \frac{v_m}{\lambda_m} B_m^b r_i - \frac{A_m^b}{2\mu_m r_i} \\ &= \frac{v_m}{\lambda_m} B_m^b r_m - \frac{A_m^b}{2\mu_m r_m} = u_{rr,i}^b \end{aligned} \tag{7.78}$$

Solving the above Eqs (7.73) ,(7.74) and (7.78), we get

$$A_i^b = \left\{\frac{2\mu_i(v_i\lambda_n - v_n\lambda_i)}{\lambda_n(2\mu_i v_i + \lambda_i)}\right\} r_n^2 \sigma_{cr} \quad \text{and} \quad B_i^b = \left\{\frac{\lambda_i(2\mu_i v_n + \lambda_n)}{\lambda_n(2\mu_i v_i + \lambda_i)}\right\} \sigma_{cr} \tag{7.79}$$

And using the value of A_i^b and B_i^b, we get

$$A_m^b = \left\{\frac{2\mu_m(v_m\lambda_i - v_i\lambda_m)}{\lambda_i(\lambda_m + 2\mu_m v_m)}\right\} r_i^2 B_i^b + \left\{\frac{\mu_m(2\mu_i v_m + \lambda_m)}{\mu_i(\lambda_m + 2\mu_m v_m)}\right\} A_i^b = \xi_b\sigma_{cr} \tag{7.80}$$

And

$$B_m^b = \left\{\frac{\lambda_m(\lambda_i + 2\mu_m v_i)}{\lambda_i(\lambda_m + 2\mu_m v_m)}\right\} B_i^b + \left\{\frac{\lambda_m(\mu_i - \mu_m)}{\mu_i(\lambda_m + 2\mu_m v_m)}\right\} \frac{A_i^b}{r_i^2} = \zeta_b\sigma_{cr} \tag{7.81}$$

where ξ_b and ζ_b defined as:

$$\xi_b = \frac{2\mu_m r_n^2}{\lambda_n}\left\{\frac{(2\mu_i\nu_m+\lambda_m)(\nu_i\lambda_n-\nu_n\lambda_i)+(\nu_m\lambda_i-\nu_i\lambda_m)(2\mu_i\nu_n+\lambda_n)\left(\frac{r_i}{r_n}\right)^2}{(2\nu_i\mu_i+\lambda_i)(2\nu_m\mu_m+\lambda_m)}\right\} \tag{7.82}$$

Similar way, we get the coefficients after debonding condition A_m^a and B_m^a, which is defined as:

$$A_m^a = \xi_a\sigma_{cr} \quad \text{and} \quad B_m^a = \zeta_a\sigma_{cr} \tag{7.83}$$

- After debonding of CNT; $\sigma_{rr,i}^a \big|_{r=r_n} = 0$,

- continuity conditions, i.e., **Fig. 7.3** as;

$$\sigma_{rr,i}^a \big|_{r=r_i} = \sigma_{rr,m}^a \big|_{r=r_i} \tag{7.84}$$

$$\zeta_b = \frac{\lambda_m}{\lambda_n}\left\{\frac{(2\mu_m\nu_i+\lambda_i)(2\mu_i\nu_n+\lambda_n)+(\mu_i-\mu_m)(\nu_i\lambda_n-\nu_n\lambda_i)\left(\frac{r_i}{r_n}\right)^2}{(2\nu_i\mu_i+\lambda_i)(2\nu_m\mu_m+\lambda_m)}\right\} \tag{7.85}$$

Applying the above-all boundary condition in Eq. (7.22) and (7.23), we find the ξ_a and ζ_a defined as:

$$\xi_a = \frac{-\mu_m}{H}\left\{\frac{(2\nu_m\mu_i\lambda_i + \lambda_m\lambda_i)r_n^2 + (2\nu_i\mu_i\lambda_m - 2\nu_m\mu_i\lambda_i)r_i^2}{\mu_i\lambda_m(2\nu_i\mu_m + \lambda_i) + \lambda_i\lambda_m(\mu_m - \mu_i)\left(\frac{r_n}{r_i}\right)^2 + 2\mu_i\mu_m(\nu_m\lambda_i - \nu_i\lambda_m)\left(\frac{r_i}{r_m}\right)^2 - \mu_m\lambda_i(2\nu_m\mu_i +}\right)$$

(7.86

$$\zeta_a = \frac{\lambda_m}{H}\left\{\frac{(2\nu_i\mu_m + \lambda_i)\mu_i + (\mu_m - \mu_i)\lambda_i\left(\frac{r_n}{r_i}\right)^2}{\mu_i\lambda_m(2\nu_i\mu_m + \lambda_i) + \lambda_i\lambda_m(\mu_m - \mu_i)\left(\frac{r_n}{r_i}\right)^2 + 2\mu_i\mu_m(\nu_m\lambda_i - \nu_i\lambda_m)\left(\frac{r_i}{r_m}\right)^2 - \mu_m\lambda_i(2\nu_m\mu_i + \lambda_m}\right)$$

(7.87